59th ILMENAU SCIENTIFIC COLLOQUIUM
Technische Universität Ilmenau, 11 – 15 September 2017
URN: urn:nbn:de:gbv:ilm1-2017iwk-040:7

A NEW APPROACH FOR HOLISTIC THREAD PROFILE DETERMINATION SUPPORTED BY OPTICAL FOCUS VARIATION MEASUREMENTS

Vinzenz Ullmann, Torsten Meß**, Kay Wenzel***, Torsten Machleidt***, Eberhard Manske**
*Technische Universität Ilmenau, Institute for Process Measurement and Sensor Technology
**Lehren- und Meßgerätewerk (LMW) Schmalkalden GmbH
***Gesellschaft für Bild- und Signalverarbeitung (GBS) mbH, Ilmenau

ABSTRACT

In this proceeding a new approach for the description of geometric-real threads will be given. The holistic determination of the virtual pitch diameter depends on the whole thread scanning. For this purpose, the optical focus variation system, consisting of a microscope objective and a digital camera, captures a stack of pictures and reconstructs the thread surface by a contrast analysis between neighbored pixels. A special calibration gauge for the focus variation system was designed and tested. The traceability and the measurement uncertainty for 3D-Points in precision thread gauge measurements will be given. The uncertainty in the current measurement setup is < 0.6 µm in each coordinate direction (x, y, z) for a S11.2 thread.

Keywords - thread parameters, thread gauges, focus variation, optical measurements, three-dimensional measurement, uncertainty and calibration

1. INTRODUCTION

In industrial precision thread fabrication and measurement processes, it is state of the art to determine thread parameters with established measurement methods like the three-wire method or the tactile profile scanning [1], [2]. With these systems the collected thread characteristic data provides only values for selected points. Therefore, a holistic description for real thread parameters is missing. One reason for that circumstance is the current thread parameter definition in engineer standards [3], [4]. Here, the thread parameter definitions refer to geometric-ideal threads. New optical measurement devices like the focus variation microscope [5], [6] will give the chance to get the whole thread surface by three-dimensional scanning. Now it is possible to overcome the limited characterization of the standards and to describe geometric-real threads aimed by a highly parallel scanning of the thread surface. The holistic characterization of a precision thread requires an adoption of the established definitions. At first, there are described the new definitions of the thread parameters like the virtual pitch diameter in chapter two. Chapter three shows the current measurement setup based on the focus variation microscope. After that, the calibration procedure for the measurement system will be explained in chapter four. Chapter five presents the traceability and the uncertainty of a captured surface point in *x*-*y*-*z*-coordinates. The uncertainty of the optical measurements will be compared to the state of the art in tactile measurements.

2. NEW DEFINITIONS OF THREAD PARAMETERS

The terms and definitions of the threads are specified in DIN 2244 [3] and ISO 5408 [4]. These definitions of thread parameters are valid for geometric-ideal threads. But in case of geometric-real threads there are some deficiencies according to a more complexity geometry.

The reasons for this circumstance are geometric differences between a real and an ideal thread. Thus, new extended definitions are created for different thread parameters including the axis of pitch diameter, the axial plane, the pitch diameter, the pitch line, the pitch cylinder, the pitch cone, the virtual pitch diameter and the pitch diameter equivalent [7]. The application of chosen definitions is shown in Figure 1.

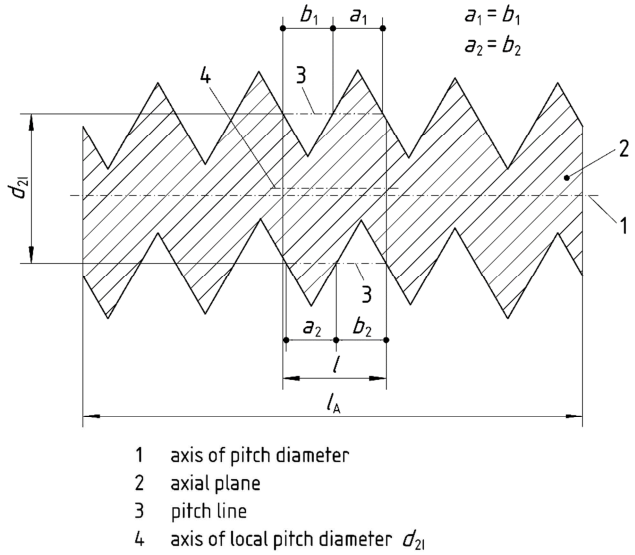

Figure 1: Screw thread elements of a cylindrical single-start thread

To describe a measured screw thread with a real geometry the first step is to calculate the axis of pitch diameter by a regression calculation (e.g. least square method). Here, the reference length l_A sets the geometrical limits for the intended thread description. But for the measurement of the local pitch diameter d_{2l} the algorithm takes the reference length l. After that, the local pitch diameter generates two pitch lines. Furthermore, the totality of all quantifiable pitch lines in the defined reference length l_A of all axial planes will describe a real pitch cylinder. A measurement process which has to realize a quantified pitch cylinder for a real thread requires a three-dimensional data set of the real thread.

3. MEASUREMENT PROCESS

3.1 Focus variation system

The implementation of the physical measuring system was realized by the GBS with the construction of a demonstrator. A sketched design of the measuring head is shown in Figure 2a. With the combination of optical tube, CCD camera and a 10x standard microscope objective, it is possible to produce the required images of a surface with a very narrow focus range. The LED light source, which is coupled into the beam path via a special optical system and the linear drive of the *t*-axis are further important components for the image stack recording. The *t*-actor is a DC motor drive with a spindle slide and an integrated incremental encoder which moves the entire optical assembly.

Measuring head**:**

- Camera: CCD, 1624 Px (H) × 768 Px (V), 30fps
- Optical tube: GBS production
- Light source: Power LED
- Objective: 10x/0.30
- *t*-axis: position range:100mm, integrated position measurement system

In addition to the measuring head, the static fixing elements and the triggered image capture system, the specially designed test specimen holder, which in turn is mounted on a cross table system, are parts of the complete design. Figure 2b is intended to illustrate this compound and the axes of motion.

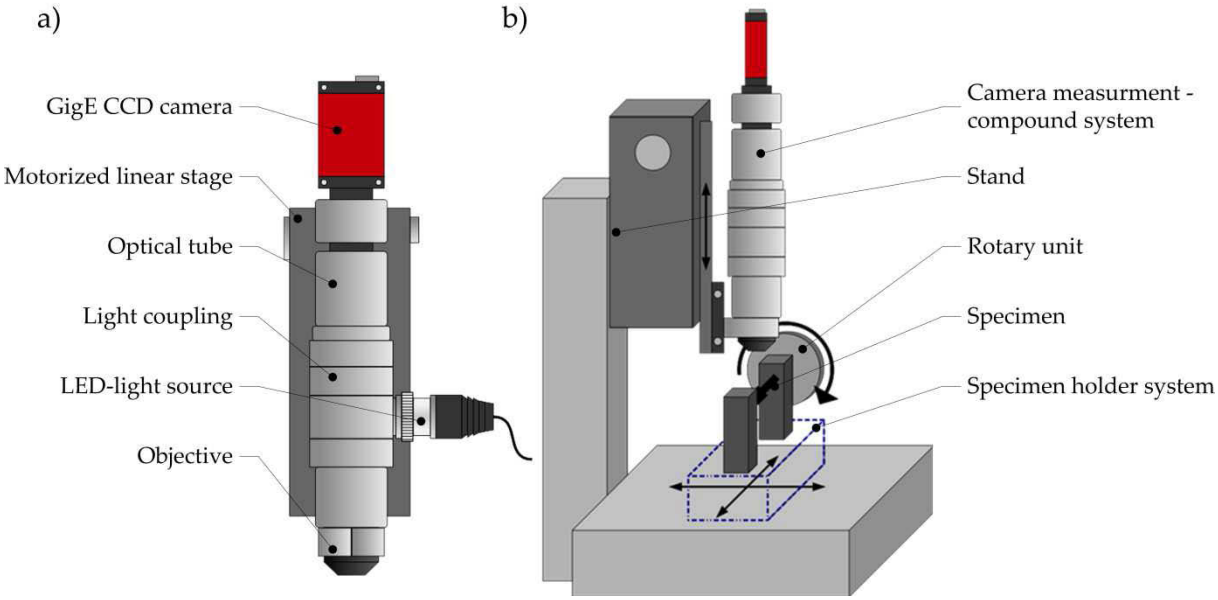

Figure 2: a) Schematic representation of the measuring head, b) overall construction of the thread measuring system

The device for clamping and aligning the measuring elements shown in Figure 3a is rigidly connected to the remaining elements. It is mounted on the cross table and provided for rotation about the *z*-axis of the thread gauges. The rotary unit can be operated either manually, with a five degree angle step width or with a motor. The snap-in device is deactivated for this purpose.
The measuring head is angularly adjustable on its carrier system in order to be able to meet different types of threads. This angle is determined exactly during the calibration process and is included in the calculations.

3.2 Data acquisition and data processing

The hardware described in section 3.1 is controlled via a specially equipped PC. The processing of the recorded data set and the subsequent evaluation of the information is also carried out via this central processing unit. The three motorized axes as well as the rotation axis are controlled by the corresponding measuring software, which also organizes the trigger synchronization and the height calculations. The focus variation was chosen as the basic measuring principle because the properties of this method have a great overlap with the system specifications. The measurement speed, resolution, angle slope and complexity of the effort correlate with the measurement requirements.
A stack of image sequences is required for the calculation of the 3D data points. The moving unit positions continuously on a ramp on the *t*-axis during the recording. The measuring system gives a trigger pulse when the next height value is reached, which follows the previous step by the preset step size. This signal triggers the camera's image recording directly. After integration and transmission from the sensor to the PC of the recorded data, the system holds the data in a buffer which can be read out and further processed by the software. The triggered mode can be executed with almost 30 fps, resulting in a measuring speed, with a step size of 1 µm, to 30 µm/s. The images are not stored on the hard disk, but they get a preprocessing

directly after recording. The process of preprocessing is worked inline while the measurement is still running. The simplest method for determining the 3D data positions, the maximum search, can also be performed simultaneously. Hence, the height information already exists after the last image has been taken. However, a more complex analysis from the preprocessed data is necessary in further steps for a more precise, stable and more meaningful indication of the heights per pixel.

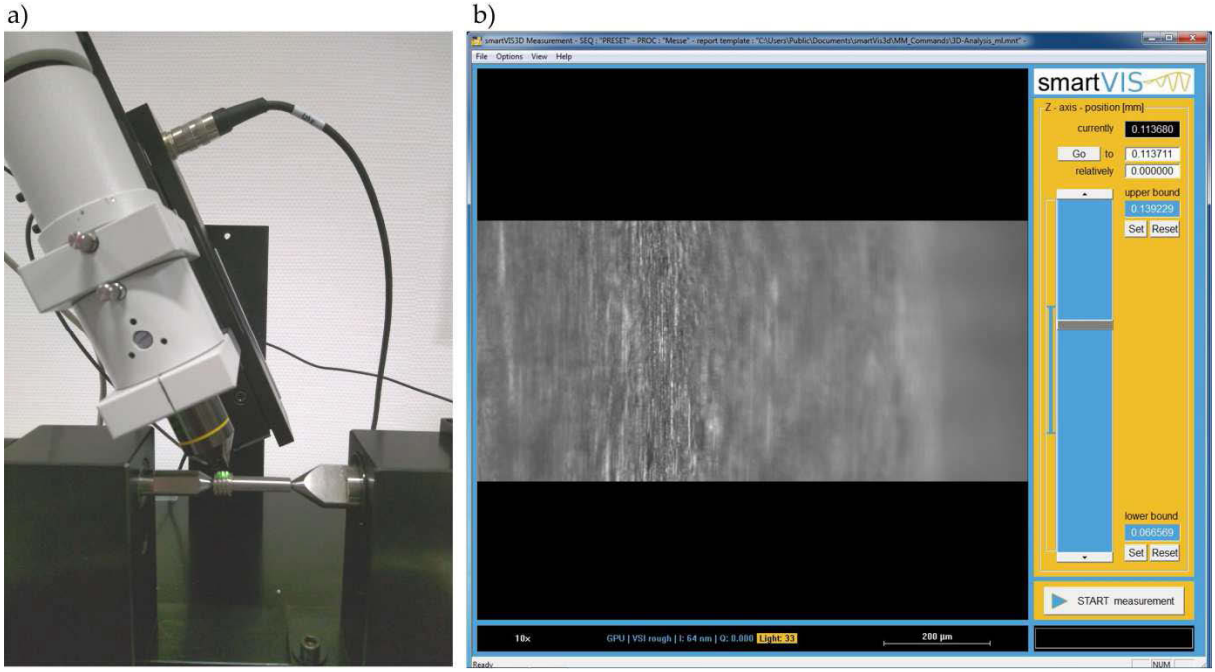

Figure 3: a) specimen holder with thread gauge and microscope objective, b) user interface, measurement and control software SmartVIS (GBS mbH)

After data acquisition, a special filter is applied to the image data (compare to Figure 4b). In principle, this is a filter associated with the family of edge detectors. Different operators have different effects to the quality and characteristics of the subsequent height evaluation.

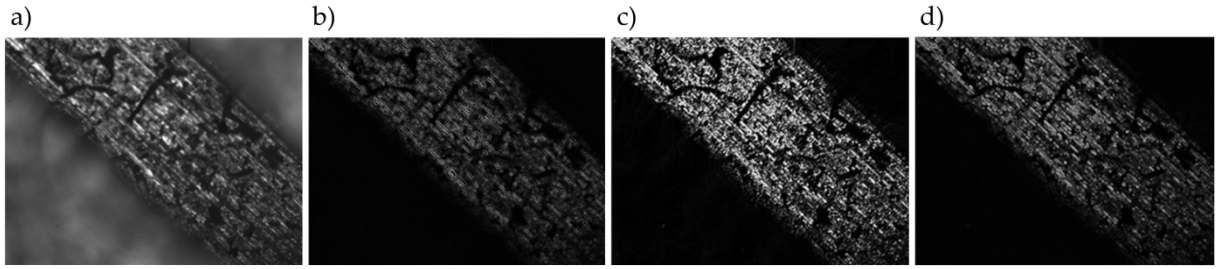

Figure 4: a) microscope image, b) with prefiltering, c) Sobel filter, d) differential filter

During preprocessing, a maximum search is applied to the filter values. The search process shifts a window over the measurement data array of each pixel. Thus, after the measurement procedure, a reduced data stack is obtained which depends on the height of the respective image point. This results in a typical course as shown in Figure 5. The *x*-axis corresponds to the number of images in the stack and the *y*-axis represents the intensity value which correlates directly with the height. These data can be imaged with a simple fitting algorithm. Preferably a normal distribution approximation is used (Normal distribution function, equation 3.1). It is possible to derive start parameters from the raw data for the approximation. Thus, the index of the maximum can be used as a starting value for the offset and the maximum itself can be used as an amplitude factor. With the method of the least error rate, a good approximation of the height values between the support points is obtained. The height

value per pixel can be read directly with the index of the maximum amplitude, which drops as a direct parameter in the method. A Gauss-Newton method can be used to find the function parameters, but other algorithms are also possible. This is the simplest method to use.

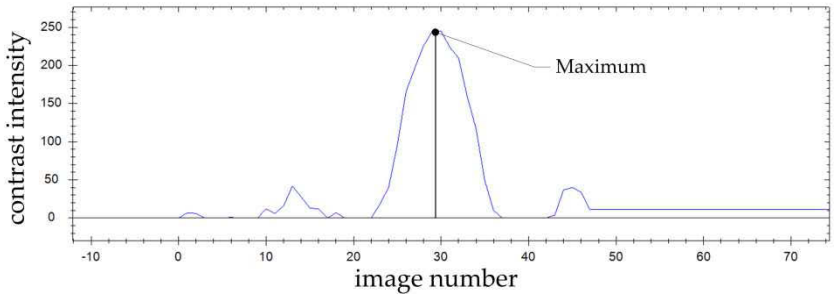

Figure 5: Intensity plot of a single pixel in the picture stack

$$f(x) = \frac{1}{\sigma\sqrt{2\pi}} e^{-\frac{1}{2}\left(\frac{x-\mu}{\sigma}\right)^2} \tag{3.1}$$

In practice, it has proven to be a good idea to use others as well. The bucket method, the matched filter or the wavelet transformation may be mentioned as examples. They all provide a higher stability in the evaluation and are suitable for practical measurements, which are usually accompanied by uncertainties.

3.3 Thread profile segmentation

After the data acquisition process, the measurement system provides filtered 2.5-dimensional parts of the thread gauge surface. For the test example with the buttress thread S11.2x2, there are 72 surface parts for one closed surface ring after scanning. Each ring has a height of h=1 mm. Five rings complete the scanned thread surface with a length of l=5 mm. Every single surface segment takes 50 megabytes of hard disk space. Hence, the full scanning data set with five rings of respectively 72 surface parts needs 18 gigabyte of hard disk space in summation. Thus, a software tool was designed for the required measurement point reduction process. At first, an algorithm transforms the data points of one surface part into the calibrated coordinate system (compare to section 4). The equations 3.2, 3.3 and 3.4 show the calculation for the x, y- and z-coordinate.

$$x = \frac{D}{2} + \cos\beta \cdot (t - p) + \frac{X}{f_x} \cdot \sin\beta \cdot \left(x_c - \frac{f_x}{2}\right) \tag{3.2}$$

$$y = \frac{Y}{f_y} \cdot \left(y_c - \frac{f_y}{2}\right) \tag{3.3}$$

$$z = z_c + \sin\beta \cdot (t - p) - \frac{X}{f_x} \cdot \cos\beta \cdot \left(x_c - \frac{f_x}{2}\right) \tag{3.4}$$

The value of D describes the diameter of the calibration gauge. β is the angle and t is the measured length position of the microscope tube. The parameter p is the calibrated reference point which describes the length position of the microscope tube axis for the intersection between the middle of focus plane and the radius of the calibration gauge surface (Figure 6). The dimensions X and Y (in mm) describe the calibrated field of view in the lines and rows of the utilized CMOS-matrix. The matrix has a resolution of $f_x = 1624$ Px and $f_y = 768$ Px. The parameters x_c and y_c are the selected position of one CMOS-matrix pixel. The dimension z_c provides the relative position of the workpiece holder with the rotary spindle under the

microscope. It is measured by the linear position system under the holder. The parameter t is the position of the microscope tube. After calculating the Cartesian coordinates x, y and z, the next step is a transformation of all data points into polar coordinates R, φ_s, and $z_p = z$. Now, the data points will be reduced in direction of the angle φ_s. The software collects only data points with a near (threshold) to a dedicated angle.

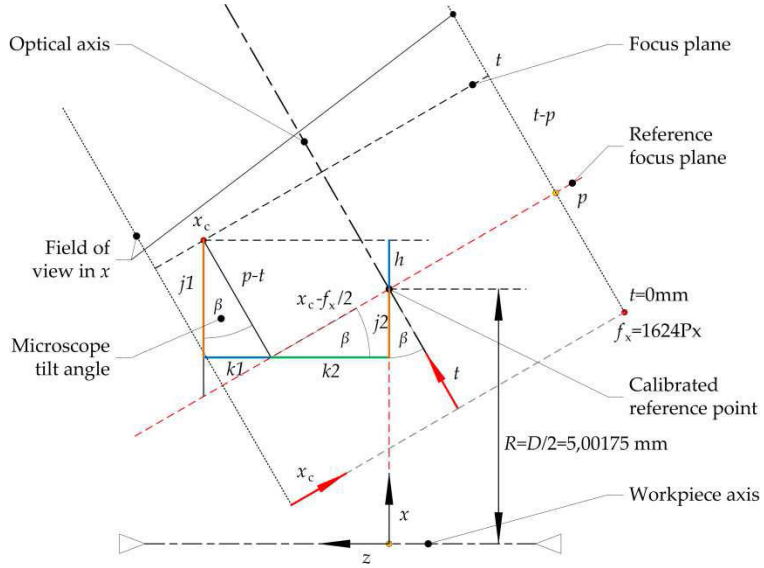

Figure 6: Defined coordinate system based on the workpiece axis, initialized by the calibration gauge

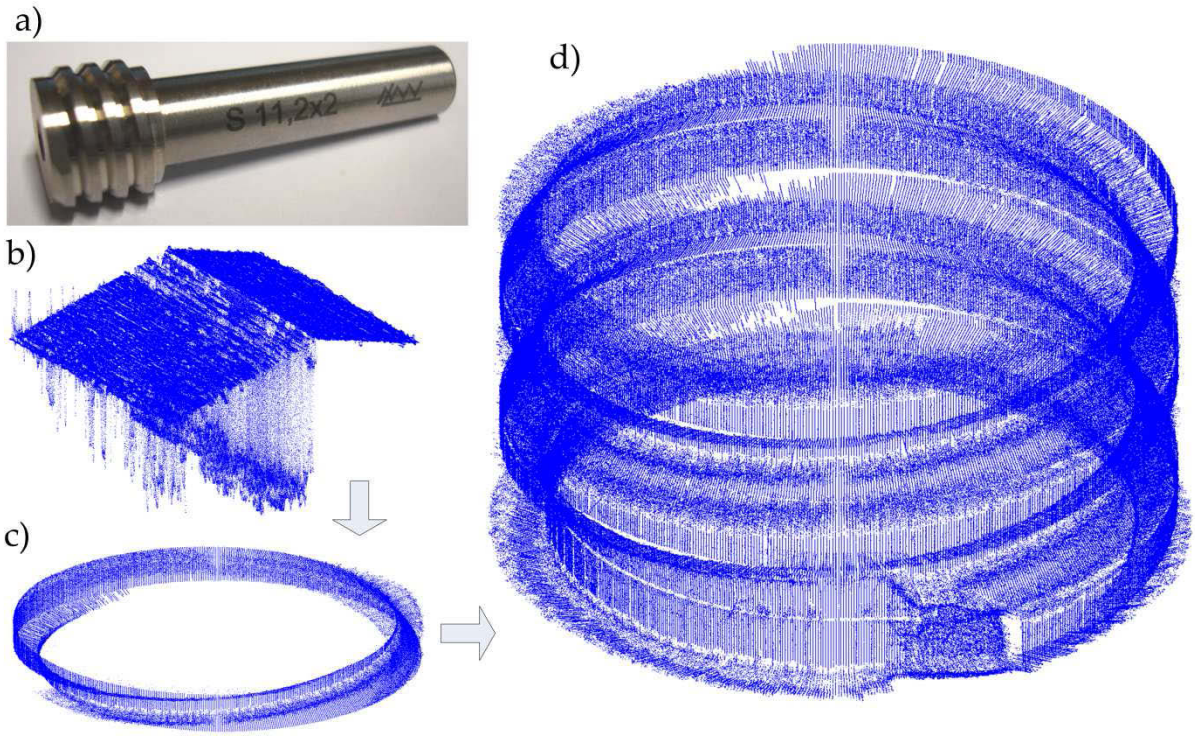

Figure 7: Focus variation results in measurements, a) test gauge S11.2x2, b) single segment with aberrations, c) ring with interpolated data points from 72 segments, d) five rings with 720 axial planes

After that, a two-dimensional linear interpolation with scattered measurement points calculates surface points along a surface line for each angle by searching and collecting three data points in the near of the searched interpolation point. Hence, the software creates a point cloud with data points at dedicated angles (compare to Figure 7). All angles in the data set

which are divided into 0.5 degree steps describe different axial planes. At this point, the whole data space consumption is reduced to less than 50 megabytes. This is a data compression factor of 1/360 and thus, the speed of the further data acquisition is increased. To calculate e.g. the pitch lines in each axial plane, the section has to be partially described by reference points in the axial plane graph. These reference points divide the thread profile into numbered increasing lines, decreasing lines, axis-parallel lines and circular arcs (see Figure 8).

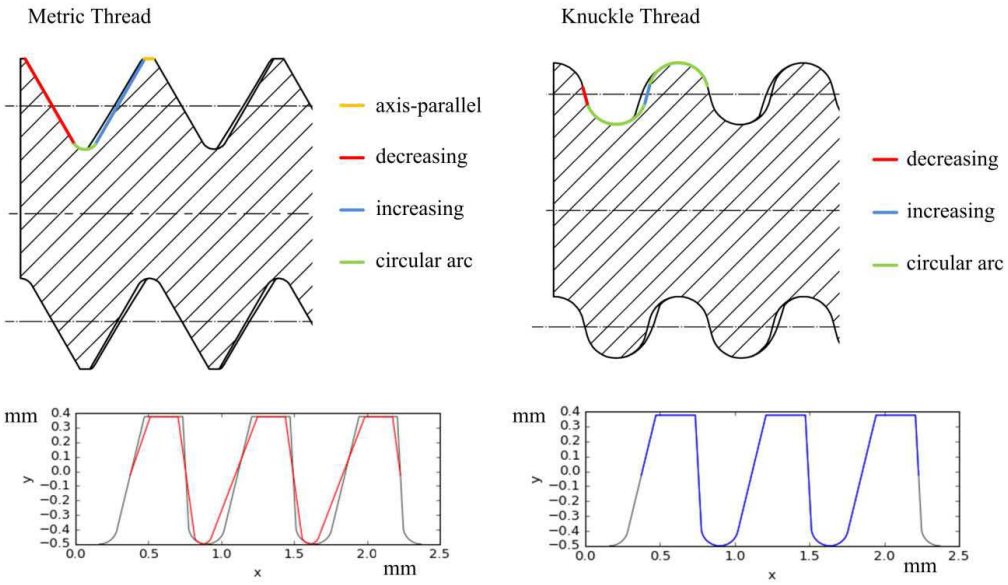

Figure 8: Thread segmentation for different thread types, geometric description by mathematical prime forms (lines, circles), according to [8]

This is important to separate the different thread teeth and gaps. After that, it is possible to calculate the pitch lines by the least square method. An analysis of the pitch lines provides the pitch diameter. In case of one axial plane every 0.5 degree, 720 different pitch diameters generate one pitch cylinder during a turn of 360°.

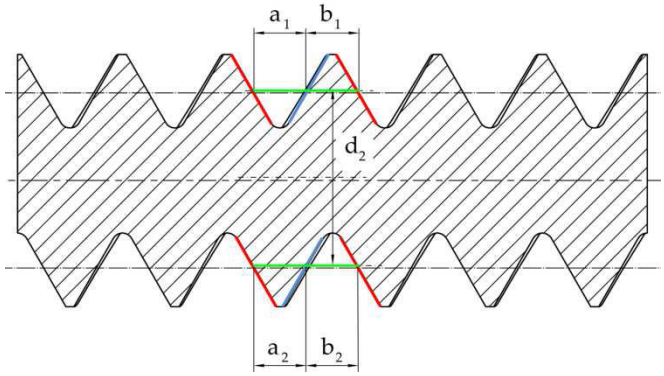

Figure 9: Fitting of one pitch line in an axial plane, the length (a) has to be equal to (b)

4. SYSTEM CALIBRATION

4.1 Calibration gauge

For the calibration of the focus variation system, a special gauge was designed and manufactured. The gauge guarantees to initialize the coordinate system of the focus variation system. Figure 10 shows the gauge and their process specified tolerances. It is very important for the calibration process to get sharp edges with a good shape quality. Thus, the fabrication processes are chosen for the best form result of the gauge surface. The sharp edges are

required to find the focus plane on the separated edges searched for. In the manufacturing sequence for sharp edges, the first step is a pre-grinding followed by a finish to decreasing the diameter down to $d = 10\,\text{mm}$. The next step is a lapping procedure for the 10 mm-diameter. Now, another grinding process generates the notches with two different gap lengths at 0.5 mm and 0.75 mm. The last step is the grinding of the bezels with a width of 0.25 mm times 45°. After the fabrication process, a measuring sequence with two systems characterizes the gauge. To measure the gap widths $M_1 = 1 \pm 0.01\,\text{mm}$ and $M_2 = 1.5 \pm 0.01\,\text{mm}$, the optical Zeiss ZKM 01-250C with an uncertainty in measurements of $u = 0.0015\,\text{mm}$ is used. A tactile Zeiss Abbé 01-200C with an uncertainty in measurements of $u = 0.00025\,\text{mm}$ determines the diameter $d = 10 \pm 0.005\,\text{mm}$ of the gauge.

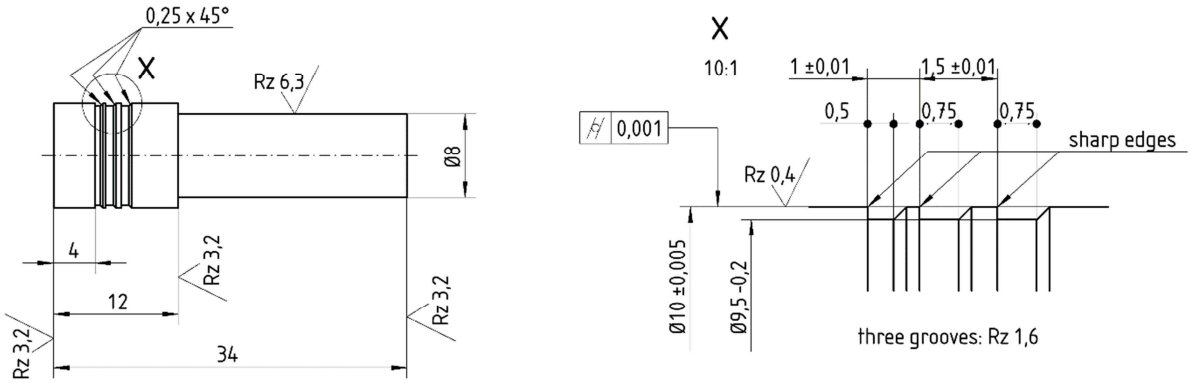

Figure 10: Calibration gauge

4.2 Calibration process

For the focus variation system calibration, the gauge is inserted between two tips of the workpiece holder. After that, the linear stage (z_c) positions the holder under the microscope in a way that one of the gauge notches is completely in the field of view.

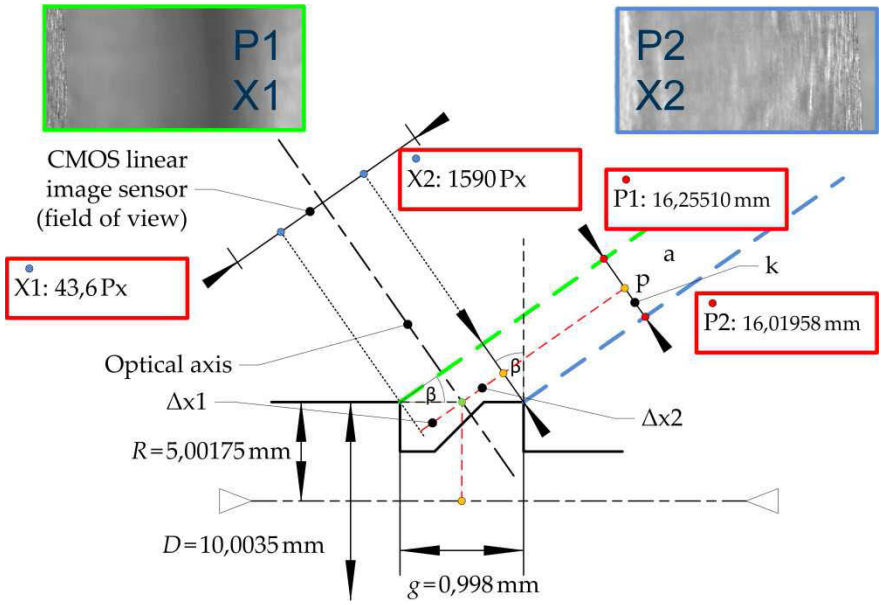

Figure 11: Optical setup in the calibration process, green box: focus on the first sharp edge, blue box: focus on the second sharp edge, red boxes: measurement example

In Figure 11, the green box shows a camera picture of the focused first sharp edge. In this position the system measures the position of the first edge X_1 in Px and the position of the linear stage for focus variation P_1 in mm. After that, the motor-driven spindle axis of the

focus variation system (t) positions the focal plane to the second sharp edge in focus. Then, the measurement system collects the values for P_2 and X_2. After that, it is possible to calculate the angle of the optical axis β and the point of intersection between the optical axis and the surface of the gauge p with the equations 4.1 and 4.2 (D=10.0035 mm, g=0.998 mm, f_x=1624 Px). f_x is the number of pixels in a line array of the camera matrix.

$$\beta = \sin^{-1}\left(\frac{P_1 - P_2}{g}\right) \tag{4.1}$$

$$p = P_2 + \frac{\left(X_2 - \frac{f_x}{2}\right) \cdot (P_1 - P_2)}{X_2 - X_1} \tag{4.2}$$

5. UNCERTAINTY IN MEASUREMENTS

5.1 Uncertainty in calibration process

The combined uncertainty of the calibrated values for β and p is described by the equation 5.1 and 5.2. The partial derivatives are based upon the equations 4.1 and 4.2.

$$u_c(\beta) = \sqrt{\left(\frac{\partial \beta}{\partial P_1} \cdot u(P_1)\right)^2 + \left(\frac{\partial \beta}{\partial P_2} \cdot u(P_2)\right)^2 + \left(\frac{\partial \beta}{\partial g} \cdot u(g)\right)^2} \tag{5.1}$$

$$u_c(p) = \sqrt{\left(\frac{\partial p}{\partial P_1} \cdot u(P_1)\right)^2 + \left(\frac{\partial p}{\partial P_2} \cdot u(P_2)\right)^2 + \left(\frac{\partial p}{\partial X_1} \cdot u(X_1)\right)^2 + \left(\frac{\partial p}{\partial X_2} \cdot u(X_2)\right)^2} \tag{5.2}$$

It is able to calculate the combined uncertainty values with the estimates of the input parameters and the uncertainty of the input parameters. The uncertainty of the input parameters is specified by ten repetitions of the calibration process. The estimated values are shown in Table 1. The measured angel of inclination between the optical axis and the work piece axis is β=13.65°±0.13° (U_{99}, k=3). The reference point is given with p=16,1381 mm±0.9 µm (U_{99}, k=3).

5.2 Uncertainty of measured surface points

The combined uncertainty of a measured 3D-datapoint in x, y and z is described by the equation 5.3, 5.4 and 5.5. The partial derivatives are based upon the equations 3.2, 3.3 and 3.4.

$$u_c(x) = \sqrt{\begin{array}{l}\left(\frac{\partial x}{\partial D} \cdot u(D)\right)^2 + \left(\frac{\partial x}{\partial \beta} \cdot u(\beta)\right)^2 + \left(\frac{\partial x}{\partial t} \cdot u(t)\right)^2 + \\ \left(\frac{\partial x}{\partial p} \cdot u(p)\right)^2 + \left(\frac{\partial x}{\partial X} \cdot u(X)\right)^2 + \left(\frac{\partial x}{\partial x_c} \cdot u(x_c)\right)^2\end{array}} \tag{5.3}$$

$$u_c(y) = \sqrt{\left(\frac{\partial y}{\partial Y} \cdot u(Y)\right)^2 + \left(\frac{\partial y}{\partial y_c} \cdot u(y_c)\right)^2} \tag{5.4}$$

$$u_c(z) = \sqrt{\left(\frac{\partial z}{\partial z_c}\cdot u(z_c)\right)^2 + \left(\frac{\partial z}{\partial \beta}\cdot u(\beta)\right)^2 + \left(\frac{\partial z}{\partial t}\cdot u(t)\right)^2 + \left(\frac{\partial z}{\partial p}\cdot u(p)\right)^2 + \left(\frac{\partial z}{\partial X}\cdot u(X)\right)^2 + \left(\frac{\partial z}{\partial x_c}\cdot u(x_c)\right)^2} \tag{5.5}$$

The estimated values are in Table 1. The values for β and p are from section 5.1. The uncertainties in measurement of the other input parameters are determined by reproducibility tests in laboratory.

Table 1: Uncertainty values for the input parameters and combined uncertainties for the output parameters, blue and red: calculated values

Input parameters			Uncertainty of output parameters	
Parameter	Estimate	Uncertainty (u)	Parameter	Combined uncertainty (u_c)
P_1	16,2551021mm	0,281µm	Calibration process	
P_2	16,0195829mm	0,563µm	β	0,548468mrad
X_1	43,6Px	0,163299Px	p	0,314µm
X_2	1590Px	0,149071Px	Measured surface points	
g	0,998mm	1,5µm	x	0,550µm
D	10,0035mm	0,25µm	y	0,329µm
t	16mm	0,36µm	z	0,547µm
X	1,01593136mm	0,437µm		
Y	0,48044045mm	0,207µm		
x_c	1Px	0,5Px		
y_c	1Px	0,5Px		
z_c	5mm	0,36µm		
β	13,65°	0,548468mrad		
p	16,1381mm	0,314µm		

In result, the x-coordinate of a data point has an uncertainty in measurement of $u = 0.550\,\mu m$. For the y-coordinate in focus variation measurements the value of a surface point has an uncertainty of $u = 0.329\,\mu m$. The uncertainty in measurement for the z-component of one data point is $u = 0.547\,\mu m$.

6. CONLUSION

New definitions of the thread parameters give the chance to describe the real geometry of a thread. For these adoptions of the norms, a focus variation measurement system is realized. Now it is possible to scan the whole surface of a geometric-real thread by combining the determined surface segments. After the generation of the whole data point cloud, different algorithms transform the data points into polar coordinates which are interpolated in z- and φ-direction. Before starting the measurements, a calibration process initializes the axes of the system aided by the use of a special designed calibration gauge. The uncertainty in measurements for one data point is $u < 0.6\,\mu m$ in each direction in space.

7. OUTLOOK

Further research steps are recommended in the future. One of these steps is the optimization of the focus variation system to reduce noise generated by glare effects on the surface under test. Another point is the reduction of the duration of the whole measurement process by increasing the scanning speed and by decreasing the time for the data acquisition steps. In the end the system requires optimized process software which includes a simple and secure handling for users, the possibility to set up the measurement parameters (e.g. reference length l_A) and a data base for different threads with their tolerances. Furthermore, it is planned to embed more thread parameters like the virtual pitch diameter and to realize the measurement of taper threads.

8. ACKNOWLEDGMENTS

Special thanks to the Bundesministerium für Wirtschaft (BMWi) and AiF for their financial support in the ZIM project EOFMEP. Thanks to the project partners GBS mbH and Lehren- und Messgerätewerk (LMW) GmbH Schmalkalden for their comprehensive support.

REFERENCES

[1] Richtlinie DKD-R 4-3, „Kalibrieren von Messmitteln für geometrische Messgrößen" Blatt 4.8 „Kalibrieren von zylindrischen Gewinde-Einstelldornen, Gewinde-Lehrdornen und –Prüfdornen", Deutscher Kalibrierdienst DKD, pp. 1-8, 06/2003.

[2] T. Primozic Merkac and B. Acko, "Comparising measuring methods of pitch diameter of thread gauges and analysis of influences on the measurement results", in: *Measurement* **43**, 2010, pp. 421-425

[3] DIN 2244: 2002-05. *Gewinde – Begriffe und Bestimmungsgrößen für zylindrische Gewinde*

[4] ISO 5408: 2009. *Screw threads – Vocabulary; Filetages - Vocabulaire*

[5] F. Helmli, R. Danzl and S. Scherer, "Optical Measurement of Micro Cutting Tools", in: *Journal of Physics: Conference Series* **311**, 2011, doi: 10.1088/1742-6596/311/1/012003

[6] T. Machleidt, D. Kapusi, K.-H. Franke and E. Manske, „Depth from focus (DFF) utilizing the large measuring volume of a nanopositioning and nanomeasuring machine", Sensoren und Messsysteme 2010 – 15. ITG/GMA-Fachtagung

[7] T. Meß, „Der Paarungsflankendurchmesser – Untersuchung des begrifflichen Umfeldes, der Einflussgrößen und der Bedeutung für die Funktion, Spezifikation, Fertigung und Prüfung von Gewinden", Dissertation, 2017, TU Ilmenau

[8] A. Dankiv, „Rechnergestützte Verarbeitung und Auswertung von Profilmessdaten optisch erfasster Gewindegeometrien", Masterarbeit, 2016, TU Ilmenau

CONTACTS

M.Sc. Vinzenz Ullmann vinzenz.ullmann@tu-ilmenau.de
Dipl.-Ing. Torsten Meß t.mess@lehrmess.de
M.Sc. Kay Wenzel Kay.wenzel@gbs-ilmenau.de
Dipl.-Ing. Torsten Machleidt torsten.machleidt@gbs-ilmenau.de
Prof. Dr.-Ing. habil. E. Manske eberhard.manske@tu-ilmenau.de